ARTICLE

doi:10.1038/nature13301

Genetics of ecological divergence during speciation

Matthew E. Arnegard[1,2], Matthew D. McGee[3], Blake Matthews[4], Kerry B. Marchinko[2], Gina L. Conte[2], Sahriar Kabir[2], Nicole Bedford[2], Sara Bergek[5]†, Yingguang Frank Chan[6], Felicity C. Jones[6], David M. Kingsley[6], Catherine L. Peichel[1] & Dolph Schluter[2]

Ecological differences often evolve early in speciation as divergent natural selection drives adaptation to distinct ecological niches, leading ultimately to reproductive isolation. Although this process is a major generator of biodiversity, its genetic basis is still poorly understood. Here we investigate the genetic architecture of niche differentiation in a sympatric species pair of threespine stickleback fish by mapping the environment-dependent effects of phenotypic traits on hybrid feeding and performance under semi-natural conditions. We show that multiple, unlinked loci act largely additively to determine position along the major niche axis separating these recently diverged species. We also find that functional mismatch between phenotypic traits reduces the growth of some stickleback hybrids beyond that expected from an intermediate phenotype, suggesting a role for epistasis between the underlying genes. This functional mismatch might lead to hybrid incompatibilities that are analogous to those underlying intrinsic reproductive isolation but depend on the ecological context.

The adaptation of populations to contrasting environments is a primary mechanism for the origin of species[1–4]. In this process, divergent selection leads to high performance of individuals exploiting alternative ecological niches through cumulative changes in potentially many traits[5]. These traits may include morphological phenotypes involved in locomotion and prey capture, behavioural traits that affect encounter rates with different prey types, and phenotypes conferring defence against niche-specific enemies[2]. The complex phenotypic basis of niche use and classic genetic models of adaptation predict that divergence in niche use will have a multilocus genetic architecture with a substantial additive component[6,7]. However, ecological divergence is often rapid and repeatable and may occur with gene flow[4], raising the possibility that niche divergence might be accomplished by a few key genomic regions[8,9]. Although the genetics of putatively adaptive traits have been widely investigated, testing these alternative predictions requires understanding of how genetic changes combine to determine whole-organism performance in different ecological niches[10,11].

Because feeding success in different trophic niches depends on an individual's phenotype and environment, we designed a new approach to evaluate predictions about its genetic basis. First we used a semi-natural setting that contained a resource distribution resembling the natural environment and allowed individuals to move freely between trophic niches. We then identified the morphological traits contributing to niche use and feeding performance, and mapped these traits genetically. To confirm that detected loci underlie trophic variation, we fitted the relationship between niche use and genotypes underlying the traits. Finally, we tested the fit of alternative genetic hypotheses of additive, dominance and epistatic effects to axes of feeding variation.

We mapped the genetic basis of niche divergence between the 'benthic' and 'limnetic' species of threespine stickleback fish (*Gasterosteus aculeatus* complex) coexisting in Paxton Lake, British Columbia, Canada. This pair of species is one of several that evolved independently in postglacial lakes in as few as 12,000 generations by adaptation to alternative niches and frequency-dependent natural selection from resource competition[12–14]. Benthic and limnetic sticklebacks show nearly complete assortative mating[15] and differ in multiple morphological traits that adapt them to contrasting inshore and pelagic lake habitats, respectively[14,16–19]. Each species pair probably arose from a double lake invasion from the sea[12], followed by further divergence with gene flow[16,20]. Hybrids are intermediate in morphology and are outperformed by each parental species in the preferred parental habitats[14,21–23]. Little intrinsic postzygotic isolation has evolved between the species: laboratory-reared hybrids are viable and fertile[16,21].

Niche use and hybrid feeding performance

Just before the breeding season in spring, we introduced 40 F_1 hybrids to an outdoor experimental pond approximating the environmental conditions and contrasting habitats of Paxton Lake (Extended Data Fig. 1 and Supplementary Discussion). We retrieved 633 F_2 hybrid juveniles before their first winter and quantified diet variation among them with the use of stable isotopes ($\delta^{13}C$ and $\delta^{15}N$; Fig. 1a). In nature, the use of open water resources by limnetic individuals gives them a lower $\delta^{13}C$ and higher $\delta^{15}N$ than the more littoral-feeding benthics, and isotope variation is correlated with foraging trait morphology[17]. Body size (length in millimetres) was our measure of F_2 hybrid feeding performance, reflecting how successfully the juveniles acquired food resources and grew during the experiment (Supplementary Discussion). Rapid attainment of adult body sizes often confers fitness advantages to sticklebacks through the effects of size on the avoidance of insect predators[24], overwinter survival[25], male resource holding potential[26] and female fecundity[14].

Under our experimental conditions, the major axis of bivariate isotope variation among F_2 hybrids (principal component 1 (PC1), hereafter

[1]Fred Hutchinson Cancer Research Center, Human Biology and Basic Sciences Divisions, 1100 Fairview Avenue North, Seattle, Washington 98109, USA. [2]University of British Columbia, Biodiversity Research Centre and Zoology Department, 6270 University Boulevard, Vancouver, British Columbia V6T 1Z4, Canada. [3]University of California at Davis, Department of Evolution and Ecology, One Shields Avenue, Davis, California 95616, USA. [4]EAWAG, Department of Aquatic Ecology, Center for Ecology, Evolution, and Biogeochemistry, Seestrasse 79, 6047 Kastanienbaum, Switzerland. [5]Uppsala University, Department of Animal Ecology, Evolutionary Biology Centre (EBC), Norbyvägen 18D, SE-75236 Uppsala, Sweden. [6]Stanford University School of Medicine, Department of Developmental Biology and Howard Hughes Medical Institute, 279 Campus Drive, Stanford, California 94305, USA. †Present address: Swedish University of Agricultural Sciences, Department of Aquatic Resources, Stångholmsvägen 2, SE-17893 Drottningholm, Sweden.

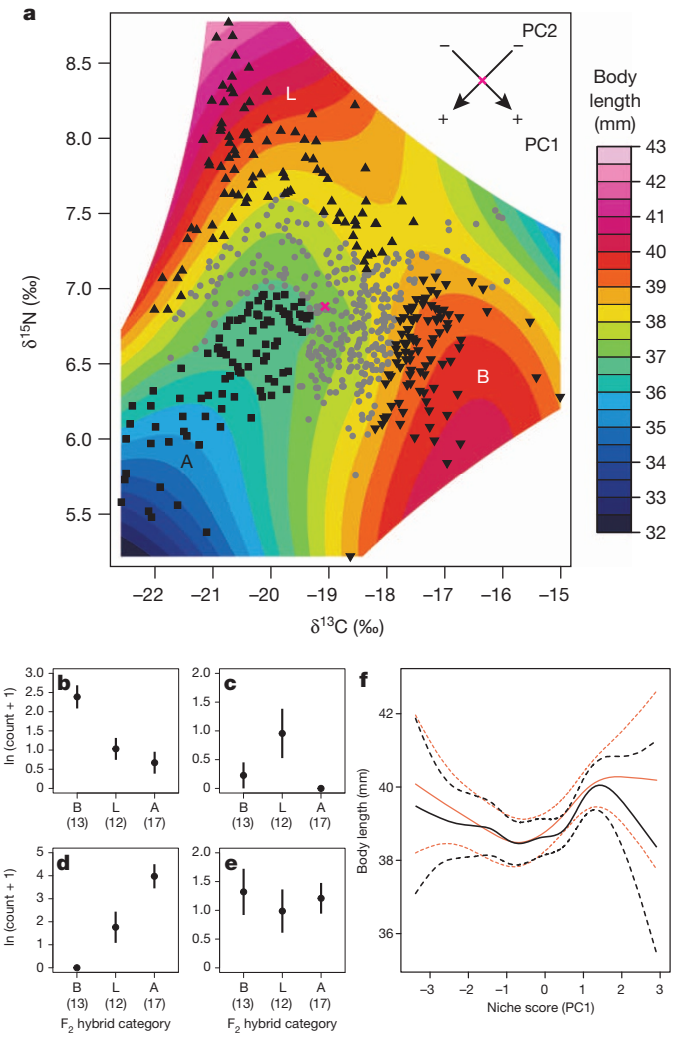

Figure 1 | Niche use and body size. **a**, Stable isotopes ($\delta^{13}C$ and $\delta^{15}N$) for 625 F_2 hybrids, showing contours of loess-smoothed body size. Individuals with extreme loess-predicted size are shown as black points (triangles point down, group B; triangles point up, group L; squares, group A; each contains 15% of individuals sampled from the pond; group L restricted to PC1 < 0.045 to preserve group distinctiveness). Other individuals are shown as grey circles. Arrows indicate principal components of isotope distribution (PC1, niche score; PC2, diet deviation score; origin, red cross). **b**–**e**, Counts of common food items (means ± 1 s.e.m.) in digestive tracts of group B, L and A individuals. **b**, Larval Chironomidae (benthic macroinvertebrate); **c**, *Skistodiaptomus oregonensis* (evasive calanoid copepod); **d**, Collembola (terrestrial origin, surface dwelling); **e**, *Chydorus* sp. (littoral cladoceran). Kruskal–Wallis tests for differences among groups: larval Chironomidae ($\chi^2_2 = 13.52$, $P = 0.001$); *S. oregonensis* ($\chi^2_2 = 7.547$, $P = 0.023$); Collembola ($\chi^2_2 = 18.67$, $P = 8.82 \times 10^{-5}$); *Chydorus* sp. ($\chi^2_2 = 0.629$, $P = 0.730$). Numbers in parentheses are values of *n*. **f**, Cubic splines[48] of mean body size against niche score (predicted values ± 2 s.e.m.) estimated with the 20 largest F_2 families ($n = 438$ individuals), 1,000 bootstrap replicates, and F_2 family as a covariate (black, all individuals; orange, individuals with PC2 < 0).

'niche score'; Fig. 1a) was consistent with the primary axis of limnetic–benthic niche divergence based on isotope data from multiple stickleback species pairs in nature[17] (Supplementary Discussion). A secondary axis of feeding variation (PC2) was also identified. To illustrate variation in phenotype and diet across isotope space, we compared recently consumed prey items among F_2 hybrids from three regions of isotope space (Fig. 1a), which we delineated using loess-predicted body size contours surrounding individuals with the largest (groups L and B) or smallest (A) average body sizes. Individuals in group B had isotope signatures resembling those of the benthic species in nature and consumed significantly more larval chironomids (Fig. 1b), on which wild benthics specialize[14,18,19]. In contrast, individuals in group L had a pelagic $\delta^{13}C$ signature and preyed most heavily on the calanoid copepod *Skistodiaptomus oregonensis* (Fig. 1c), a key planktonic prey item on which limnetics are specialized[14,17,19]. The small F_2 hybrids in group A fed predominantly on a symphypleonan springtail species (Fig. 1d), which is not a major dietary component of benthics or limnetics in the native lakes[14,17]. We therefore refer to PC2 as 'diet deviation score' because it reflects variation independent of the typical limnetic–benthic feeding axis. The groups did not differ in their consumption of *Chydorus* sp., a littoral cladoceran (Fig. 1e). Additional analyses of consumed prey using all F_2 individuals confirmed these feeding patterns (Extended Data Fig. 2 and Supplementary Discussion).

Analysis of the variation in juvenile size across the entire isotope space revealed a saddle-shaped landscape (Fig. 1a). F_2 hybrids exploiting either the limnetic (group L) or benthic (group B) extremes of the isotope distribution grew more than the other F_2 hybrids, which either had intermediate niche scores and diets or exhibited an alternative feeding pattern (group A). In nature, benthics grow to a larger adult size than limnetics[14,16], in part because they differ in the age of sexual maturity[27]; however, in our experiment, mean body size was similar between the F_2 hybrids in groups B and L (Fig. 1a). This finding might have resulted from sampling the experimental fish as juveniles or from resource abundance differences between the experimental pond and Paxton Lake. The body size valley at intermediate niche scores (Fig. 1a) persists when F_2 family identity is included as a covariate, which controls for variation in F_2 hatching date and hence fish age (Fig. 1f). Considering the 20 largest F_2 families, niche score was reasonably well fitted by a quadratic regression model including the family covariate ($R^2 = 33.2\%$; $F_{21,416} = 9.847$; $P < 2.20 \times 10^{-16}$). Although we found only suggestive evidence for a positive quadratic term in this model (coefficient estimate = 0.173 ± 0.101 s.e.m.; $P = 0.086$; Supplementary Discussion), within-family regression revealed that 16 families individually showed positive quadratic coefficients, indicating that the dip in body size at intermediate niche score is statistically significant ($P = 0.012$; two-sided binomial test). Overall, these results support the hypothesis that F_2 hybrids with an intermediate trophic phenotype suffered a growth disadvantage.

Morphological basis of niche divergence

Many phenotypic traits contribute to niche score variation. To determine this we measured nine functional morphological traits that are important in prey capture and retention, including craniofacial traits affecting the capacity to generate suction pressure, the speed and extent of jaw protrusion, and the retention of ingested prey items (Fig. 2)[16–19]. We additionally measured the *x* and *y* coordinates of 19 morphological landmarks indicating body and head shape[28] (Extended Data Fig. 3), which are expected to influence feeding performance. We used all-subsets linear regression to test effects of functional morphological traits and body shape coordinates, separately, on niche score. The best functional trait models (with a difference in Akaike information criterion (ΔAIC; see Methods) of between 0 and 2) fitting niche score contained terms for three of the five components of the suction feeding index[18], two key oral jaw traits[19] and both gill raker counts[16,17] (Supplementary Table 1). The best models fitting niche score to body shape contained terms for 22 of 38 landmark coordinates[28] (Supplementary Table 2). Hereafter, we consider the traits included in the best models to be 'component traits' of niche divergence between Paxton benthics and limnetics.

Genetic architecture of niche divergence

We conducted quantitative trait locus (QTL) mapping on all measured morphological traits and found 76 significant QTLs, including 41 QTLs for 19 of the 29 component traits. The QTLs show small to moderate phenotypic effect sizes (Supplementary Table 3). Component trait QTLs occur on 14 of the 21 linkage groups (LGs) in the threespine stickleback genome[29] (Extended Data Fig. 3), suggesting that multiple genetic factors contribute to niche divergence between Paxton benthics and limnetics. Both among LGs and within certain LGs, we find significant

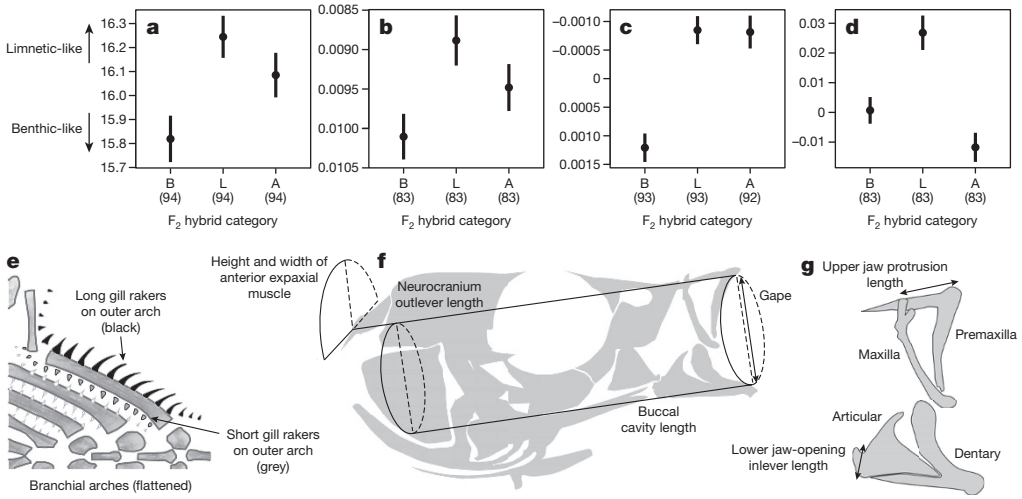

Figure 2 | Trait variation among F_2 hybrid groups. **a**–**d**, Trait means (± 1 s.e.m.) of F_2 hybrids in categories B, L and A (Fig. 1a): **a**, number of short gill rakers (ANOVA, $F_{2,279} = 5.396$, $P = 0.005$); **b**, suction feeding index ($F_{2,246} = 4.080$, $P = 0.018$); **c**, residual lower jaw-opening inlever length ($F_{2,275} = 20.36$, $P = 5.65 \times 10^{-9}$); **d**, residual upper jaw protrusion length ($F_{2,246} = 14.94$, $P = 7.54 \times 10^{-7}$). Numbers in parentheses are values of *n*. Arrows indicate directions of benthic–limnetic divergence (vertical axes of **b** and **c** are inverted to facilitate visual comparisons). **e**–**g**, Trait illustrations: **e**, gill rakers, functioning in prey retention[16,17]; **f**, five components of suction feeding index[18,19]; **g**, two oral jaw traits that influence efficiency of capturing evasive zooplankton[19].

clustering of co-localized QTLs (Extended Data Table 1 and Supplementary Discussion), indicating close linkage or pleiotropic effects of genes underlying different component traits of niche use. Nearly all QTLs for the component traits occur in known regions of repeated genomic differentiation between sympatric benthic and limnetic species in multiple lakes[30].

To determine how these QTLs contribute to benthic–limnetic niche divergence, we fitted multiple-QTL mapping (MQM) models of niche score to genotypes at QTLs for component traits. We selected only the single morphological QTL with the strongest estimated effect on niche score from each of the 14 LGs containing QTLs for component traits. Although this method is conservative and may underestimate the number of loci underlying niche score, it avoids unduly complex models involving multiple linked loci within LGs. We found additive allelic effects across multiple loci (Fig. 3). Seven of the 14 selected QTLs significantly affected niche score (Extended Data Table 2). Two of these loci resided within clusters of co-localized QTLs on LGs 4 and 16 (Extended Data Fig. 3, Extended Data Table 1 and Supplementary Discussion). However, effect sizes were distributed roughly evenly among the seven significant loci (percentage of total variance explained = 1.16–3.74%; Extended Data Table 2). Next, we allowed all significant pairwise QTL × QTL interactions to enter the model and followed this by backward elimination of non-significant terms. The resulting 'full' MQM model contained four pairwise interactions in addition to main effects representing 11 of the 14 morphological QTLs (Extended Data Table 3).

To test the relative contributions of additive, dominance and pairwise epistatic effects of these loci to niche score, we specified and compared three nested, general linear models at the markers nearest to the 11 significant QTL positions in the full MQM model. The 'additive' model contained only the additive effects of the 11 loci (Fig. 3b; adjusted $R^2 = 15.8\%$; $F_{39,484} = 3.514$; $P = 5.76 \times 10^{-11}$; AIC = 1,533.42). By contrast, the 'additive + dominance' model contained both additive and dominance effects of these loci (adjusted $R^2 = 14.4\%$; $F_{50,473} = 2.763$; $P = 1.18 \times 10^{-8}$; AIC = 1,551.80). On the basis of AIC, adjusted R^2, and results of a likelihood ratio (G) test, we conclude that dominance does not contribute significantly to the additive genetic model for niche score ($G_{(\text{add+dom, add})} = 3.625$; $P = 0.980$). However, the 'full' model, with all additive and dominance effects across the 11 loci as well as the four significant pairwise epistatic interactions (Fig. 3c; adjusted $R^2 = 20.6\%$; $F_{66,457} = 3.059$; $P = 2.75 \times 10^{-12}$; AIC = 1,526.37), provides a significantly better fit to the data than the additive model ($G_{(\text{full, add})} = 61.05$; $P = 1.92 \times 10^{-4}$) or the additive + dominance model ($G_{(\text{full, add+dom})} = 57.43$; $P = 1.41 \times 10^{-6}$). These results verify the prediction of a polygenic and largely additive basis to whole-organism niche use. F_2 hybrids that grew the most during our study, reflecting high feeding performance, were either those individuals with the highest number of limnetic alleles across loci and the most limnetic-like phenotype and diet, or the highest number of benthic alleles and the most benthic-like phenotype and diet (Figs 1b, c, 2a–d and 3a and Extended Data Figs 2, 4–6). Pairwise genetic interactions also had a significant, although smaller, effect on niche score (compare Fig. 3b with Fig. 3c). This is consistent with a role for epistasis in adaptation, although the importance of epistasis may be underestimated because genetic interactions can be difficult to detect, particularly when they are weak or involve more than two interacting genetic factors[31,32].

Trait mismatch reduces growth

Analysis of the secondary axis of isotope variation, the diet deviation score, provided additional evidence for non-additive effects. Inspection of phenotypes of hybrids in group A suggests that this subset of individuals experienced growth deficits (Fig. 1a) due to functional mismatch between certain traits. These group A individuals had distinctly limnetic-like lower jaw-opening inlevers (Fig. 2c, g), which contributed to the rapid jaw opening needed for successful strikes on evasive zooplankton such as *S. oregonensis*[19]. Yet they also had reduced, or benthic-like, upper jaw protrusion (Fig. 2d, g), which is expected to decrease the efficiency of zooplanktivory[19]. The F_2 hybrids in group A also exhibited mismatches in other combinations of traits (Fig. 2a, Extended Data Figs 4 and 5 and Supplementary Discussion). We predict that these conflicting trait combinations would reduce an individual's foraging success in both parental habitats, which could explain why these hybrids, as a group, were the smallest of any phenotypic class (Fig. 1a). This phenotypic interaction would imply epistasis for performance at underlying genes even if the phenotypic traits themselves have a largely additive genetic basis[33]. Such epistatic effects are expected to be manifested only in environments containing the divergent habitats to which the parental populations are adapted.

To investigate further, we applied the approach used in our genetic analysis of niche score to diet deviation score. Although many morphological traits underlie variation along this secondary feeding axis, MQM modelling revealed no statistically significant relationship between the

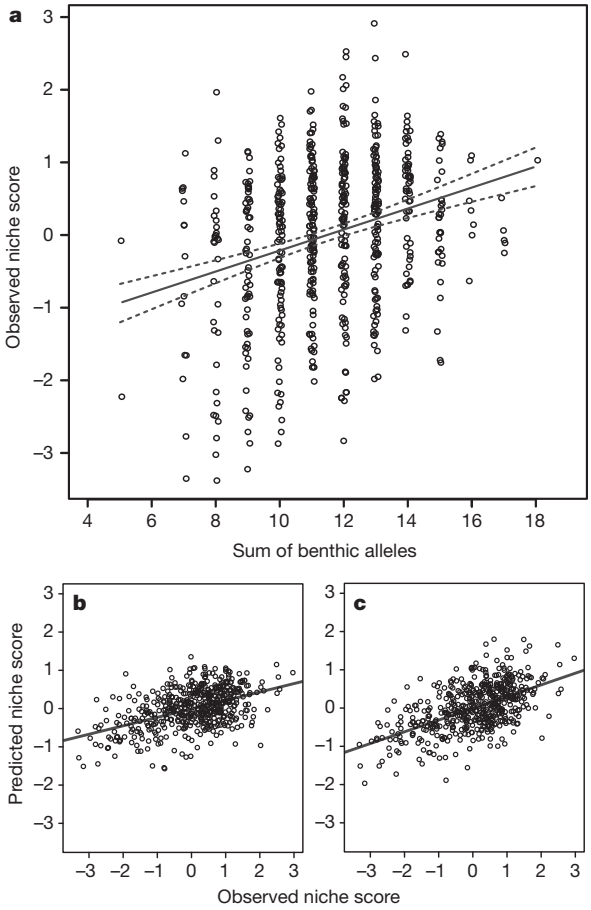

Figure 3 | Genetic architecture of niche divergence. **a**, Niche scores of F_2 hybrids are predicted from the number of benthic alleles summed across 11 unlinked loci in the full MQM model ($R^2 = 0.081$; $F_{1,605} = 53.52$; $P = 8.18 \times 10^{-13}$). Dashed lines are 95% confidence intervals of regression line (solid). **b**, Observed niche score compared with that predicted by the additive-only genetic model. **c**, Observed niche score compared with that predicted by the full genetic model: additive, dominance and epistatic effects. Statistics for **b** and **c** are provided in the text.

QTLs for these traits and diet deviation score. Consequently, we focused on strongest-effect QTLs for the two traits that showed clear phenotypic mismatch in group A individuals (Fig. 2c, d), had strong effects on niche score (Extended Data Fig. 6 and Supplementary Table 1) and were among the most divergent functional morphological phenotypes known in the species pair[19] (that is, the QTLs at 28.8 centimorgans (cM) on LG 4 for lower jaw-opening inlever, and 28.4 cM on LG 9 for upper jaw protrusion; Supplementary Table 3). Using genotypes at the marker nearest to each of these QTLs, we found suggestive evidence of negative epistasis underlying diet deviation score in a two-way analysis of variance (ANOVA) of all F_2 individuals (interaction term: $F_{4,598} = 2.254$; $P = 0.0621$).

Discussion

Although early in the speciation process, Paxton limnetic and benthic sticklebacks differ in many morphological traits. We show that many of these divergent traits contribute to variation in niche use and growth of juvenile F_2 hybrids foraging freely in a semi-natural environment. Multiple genetic factors with largely additive effects, distributed across many chromosomes, underlie niche divergence along the limnetic–benthic resource gradient. Replacement of a limnetic allele by a benthic allele (or vice versa) at any of these loci shifts the niche score in hybrids by roughly the same magnitude (Fig. 3a). We also found evidence for a functional mismatch between phenotypic traits in hybrids that adopted an alternative feeding mode, accompanied by the slowest growth in the mapping population. This suggests that when multiple traits must function together, novel combinations of traits in hybrids might reduce performance below that expected for an intermediate phenotype. We predict that similar genetic architectures—involving multiple genomic regions each with a relatively small effect, coupled with the possibility of functional mismatch of some gene combinations—will be found for other complex, whole-organism phenotypes that depend on many component traits.

Our finding that niche divergence is determined by small-effect loci on more than half of the chromosomes in the threespine stickleback genome might not be expected in systems in which gene flow still occurs. Theory indicates that loci with relatively large effect sizes under the strongest divergent selection will most readily resist gene flow[9], and these loci would be detected most readily by QTL mapping. In contrast, loci under weak divergent selection are less able to resist gene flow unless they are sufficiently tightly linked to other loci under sufficiently strong selection[9,34]. Nevertheless, our results are consistent with genome scans of ecologically divergent populations of several organisms, including threespine sticklebacks, which typically show differences in many regions distributed across the genome[29,30,35–38]. It is possible that the broadly distributed genetic architecture of niche divergence in the Paxton Lake species pair has arisen from strong, multifarious divergent selection[39] acting simultaneously on the numerous traits that underlie adaptation to open-water versus littoral or benthic habitats. Another intriguing possibility is that this broadly distributed genetic architecture results from segregation of ancestral variation that arose during periods of allopatry[30,38,40].

Our results contribute to an understanding of the genetics of environment-dependent reproductive isolation during ecological speciation, because divergence in traits underlying niche use reduces the fitness of intermediate phenotypes, including hybrids, when intermediate environments are uncommon or unprofitable[22,41,42]. Environment-dependent reproductive isolation accompanies the earliest stages of adaptation and may drive the evolution of additional forms of reproductive isolation[2,43]. If rapid growth of certain threespine stickleback juveniles (such as those in groups L and B) has positive consequences for fitness, then disruptive selection found in the saddle-shaped landscape of body size (Fig. 1a) might reflect selection against intermediate hybrid phenotypes along the major axis of niche differentiation (Fig. 1f). This pattern corroborates the results from transplant experiments in the native lake showing a growth disadvantage in intermediate hybrids relative to the two parental species in their native habitats[14,21,22]. Thus, our results on the genetics of divergence in niche use and whole-organism performance suggest that the underlying genetic basis of extrinsic postzygotic reproductive isolation between limnetic and benthic sticklebacks is largely additive. This contrasts with the genetics of environment-independent or 'intrinsic' postzygotic isolation, the evolution of which is well described by the Bateson–Dobzhansky–Muller model and is largely caused by negative epistatic interactions between loci[3,8,44]. Nevertheless, our results show that a mismatch of oral jaw traits reduces feeding performance of some F_2 hybrid sticklebacks beyond that expected from additive genetic effects alone. A functional mismatch between traits might therefore represent an environment-dependent counterpart to the deleterious intermolecular interactions often associated with intrinsic postzygotic isolation[44]. As our results suggest, hybrids that are phenotypically mismatched for ecological performance traits may be produced inevitably as the process of ecological speciation unfolds, thereby contributing to the further evolution of reproductive isolation.

METHODS SUMMARY

We established four F_1 families from crosses between unique wild benthic and limnetic F_0 individuals. On 17 March 2008 we added five adults of each sex and F_1 family to an experimental pond at the University of British Columbia. The 40 F_1 hybrids mated freely to produce a large F_2 intercross population. From 5 to 21 October 2008 we collected and euthanized 633 F_2 juveniles and measured stable carbon and nitrogen isotopes in samples of axial muscle[17,45]. Prey items were counted in the digestive tracts of 99 of these individuals[14]. We analysed body shape with 19

morphometric landmarks placed on images of all fixed and stained individuals[28]. We also measured nine traits functioning in prey capture or retention[16–19]. Using all-subsets linear regression, we identified 'component traits' that predict variation along principal component 1 (PC1; niche score) or 2 (PC2; diet deviation score) of the stable-isotope distribution. We genotyped F_0, F_1 and F_2 individuals at 408 single-nucleotide polymorphisms (SNPs)[30] and used JoinMap 3.0[46] to construct a linkage map. Data from 530 individuals in the 29 F_2 families containing at least eight full sibs each were used to interval map traits in R/qtl with Haley–Knott regression and F_2 family as a covariate[47]. Genome-wide LOD significance thresholds ($\alpha = 0.05$) were estimated by permutation (10,000 iterations per trait). One QTL on each LG with the greatest estimated effect on PC1 (or PC2) was identified as the highest-LOD QTL among component traits mapping to that LG. We tested how the identified QTLs affected either trophic axis by fitting MQM models for PC1 or PC2 with Haley–Knott regression and the F_2 family covariate[47]. Additive, dominance and pairwise epistatic effects in the final MQM model for PC1 were tested with nested general linear models and compared using AIC, adjusted R^2, and likelihood ratio tests.

Online Content Methods, along with any additional Extended Data display items and Source Data, are available in the online version of the paper; references unique to these sections appear only in the online paper.

Received 4 June 2013; accepted 1 April 2014.
Published online 8 June 2014.

1. Darwin, C. *The Origin of Species by Means of Natural Selection* (John Murray, 1859).
2. Schluter, D. *The Ecology of Adaptive Radiation* (Oxford Univ. Press, 2000).
3. Coyne, J. A. & Orr, H. A. *Speciation* (Sinauer Associates, 2004).
4. Nosil, P. *Ecological Speciation* (Oxford Univ. Press, 2012).
5. Chase, J. M. & Leibold, M. A. *Ecological Niches: Linking Classical and Contemporary Approaches* (Univ. of Chicago Press, 2003).
6. Fisher, R. A. *The Genetical Theory of Natural Selection* (Oxford Univ. Press, 1930).
7. Orr, H. A. The genetic theory of adaptation: a brief history. *Nature Rev. Genet.* **6,** 119–127 (2005).
8. Gavrilets, S. *Fitness Landscapes and the Origin of Species* (Monographs in Population Biology Vol. 41, Princeton Univ. Press, 2004).
9. Yeaman, S. & Whitlock, M. C. The genetic architecture of adaptation under migration-selection balance. *Evolution* **65,** 1897–1911 (2011).
10. Mackay, T. F. C., Stone, E. A. & Ayroles, J. F. The genetics of quantitative traits: challenges and prospects. *Nature Rev. Genet.* **10,** 565–577 (2009).
11. Barrett, R. D. H. & Hoekstra, H. E. Molecular spandrels: tests of adaptation at the genetic level. *Nature Rev. Genet.* **12,** 767–780 (2011).
12. Taylor, E. B. & McPhail, J. D. Historical contingency and ecological determinism interact to prime speciation in sticklebacks, *Gasterosteus*. *Proc. R. Soc. Lond. B* **267,** 2375–2384 (2000).
13. Schluter, D. Experimental evidence that competition promotes divergence in adaptive radiation. *Science* **266,** 798–801 (1994).
14. Schluter, D. Adaptive radiation in sticklebacks: trade-offs in feeding performance and growth. *Ecology* **76,** 82–90 (1995).
15. Rundle, H. D., Nagel, L. N., Boughman, J. W. & Schluter, D. Natural selection and parallel speciation in sympatric sticklebacks. *Science* **287,** 306–308 (2000).
16. McPhail, J. D. Ecology and evolution of sympatric sticklebacks (*Gasterosteus*): evidence for a species pair in Paxton Lake, Texada Island, British Columbia. *Can. J. Zool.* **70,** 361–369 (1992).
17. Matthews, B., Marchinko, K. B., Bolnick, D. I. & Mazumder, A. Specialization of trophic position and habitat use by sticklebacks in an adaptive radiation. *Ecology* **91,** 1025–1034 (2010).
18. McGee, M. D. & Wainwright, P. C. Convergent evolution as a generator of phenotypic diversity in threespine stickleback. *Evolution* **67,** 1204–1208 (2013).
19. McGee, M. D., Schluter, D. & Wainwright, P. C. Functional basis of ecological divergence in sympatric stickleback. *BMC Evol. Biol.* **13,** 277 (2013).
20. Gow, J. L., Peichel, C. L. & Taylor, E. B. Contrasting hybridization rates between sympatric three-spined sticklebacks highlight the fragility of reproductive barriers between evolutionarily young species. *Mol. Ecol.* **15,** 739–752 (2006).
21. Hatfield, T. & Schluter, D. Ecological speciation in sticklebacks: environment-dependent hybrid fitness. *Evolution* **53,** 866–873 (1999).
22. Rundle, H. D. A test of ecologically dependent postmating isolation between sympatric sticklebacks. *Evolution* **56,** 322–329 (2002).
23. Gow, J. L., Peichel, C. L. & Taylor, E. B. Ecological selection against hybrids in natural populations of sympatric threespine sticklebacks. *J. Evol. Biol.* **20,** 2173–2180 (2007).
24. Marchinko, K. B. Predation's role in repeated phenotypic and genetic divergence of armor in threespine stickleback. *Evolution* **63,** 127–138 (2009).
25. Carlson, S. M., Kottas, A. & Mangel, M. Bayesian analysis of size-dependent overwinter mortality from size-frequency distributions. *Ecology* **91,** 1016–1024 (2010).
26. Candolin, U. & Voigt, H.-R. Correlation between male size and territory quality: consequence of male competition or predation susceptibility? *Oikos* **95,** 225–230 (2001).
27. MacColl, A. D. C. Parasites may contribute to 'magic trait' evolution in the adaptive radiation of three-spined sticklebacks, *Gasterosteus aculeatus* (Gasterosteiformes: Gasterosteidae). *Biol. J. Linn. Soc.* **96,** 425–433 (2009).
28. Rogers, S. M. *et al.* Genetic signature of adaptive peak shift in threespine stickleback. *Evolution* **66,** 2439–2450 (2012).
29. Jones, F. C. *et al.* The genomic basis of adaptive evolution in threespine sticklebacks. *Nature* **484,** 55–61 (2012).
30. Jones, F. C. *et al.* A genome-wide SNP genotyping array reveals patterns of global and repeated species-pair divergence in sticklebacks. *Curr. Biol.* **22,** 83–90 (2012).
31. Phillips, P. C. Epistasis—the essential role of gene interactions in the structure and evolution of genetic systems. *Nature Rev. Genet.* **9,** 855–867 (2008).
32. Mackay, T. F. C. Epistasis and quantitative traits: using model organisms to study gene–gene interactions. *Nature Rev. Genet.* **15,** 22–33 (2014).
33. Whitlock, M. C., Phillips, P. C., Moore, F. B.-G. & Tonsor, S. J. Multiple fitness peaks and epistasis. *Annu. Rev. Ecol. Syst.* **26,** 601–629 (1995).
34. Via, S. Natural selection in action during speciation. *Proc. Natl Acad. Sci. USA* **106,** 9939–9946 (2009).
35. Hohenlohe, P. A. *et al.* Population genomics of parallel adaptation in threespine stickleback using sequenced RAD tags. *PLoS Genet.* **6,** e1000862 (2010).
36. Feder, J. L., Egan, S. P. & Nosil, P. The genomics of speciation-with-gene-flow. *Trends Genet.* **28,** 342–350 (2012).
37. Strasburg, J. L. *et al.* What can patterns of differentiation across plant genomes tell us about adaptation and speciation? *Phil. Trans. R. Soc. B* **367,** 364–373 (2012).
38. Seehausen, O. *et al.* Genomics and the origin of species. *Nature Rev. Genet.* **15,** 176–192 (2014).
39. Rice, W. R. & Hostert, E. E. Laboratory experiments on speciation: what have we learned in 40 years? *Evolution* **47,** 1637–1653 (1993).
40. Schluter, D. & Conte, G. L. Genetics and ecological speciation. *Proc. Natl Acad. Sci. USA* **106,** 9955–9962 (2009).
41. Egan, S. P. & Funk, D. J. Ecologically dependent postmating isolation between sympatric host forms of *Neochlamisus bebbianae* leaf beetles. *Proc. Natl Acad. Sci. USA* **106,** 19426–19431 (2009).
42. McBride, C. S. & Singer, M. C. Field studies reveal strong postmating isolation between ecologically divergent butterfly populations. *PLoS Biol.* **8,** e1000529 (2010).
43. Rundle, H. D. & Nosil, P. Ecological speciation. *Ecol. Lett.* **8,** 336–352 (2005).
44. Presgraves, D. C. The molecular evolutionary basis of species formation. *Nature Rev. Genet.* **11,** 175–180 (2010).
45. Fry, B. *Stable Isotope Ecology* (Springer, 2006).
46. van Ooijen, J. W. & Voorrips, R. E. *JoinMap® 3.0: Software for the Calculation of Genetic Linkage Maps* (Plant Research International, 2001).
47. Broman, K. W. & Sen, S. *A Guide to QTL Mapping with R/qtl* (Springer Science+Business Media, 2009).
48. Schluter, D. Estimating the form of natural selection on a quantitative trait. *Evolution* **42,** 849–861 (1988).

Supplementary Information is available in the online version of the paper.

Acknowledgements We thank J. Perez for counting gill rakers; C. Sather for performing lab work for SNP genotyping; and K. Broman, G. Coop, I. Goodliffe, A. Greenwood, P. Wainwright, M. White and M. Wund for constructive comments. Stable isotopes were analysed at the University of California, Davis, Stable Isotope Facility. Funding was provided by grants from the US National Institutes of Health (F32 GM086125 to M.E.A., R01 GM089733 to C.L.P. and D.S., and P50 HG002568 to C.L.P. and D.M.K.), the Natural Sciences and Engineering Research Council of Canada (to D.S.) and the Canada Foundation for Innovation (to D.S.).

Author Contributions M.E.A., C.L.P. and D.S. designed, planned and oversaw the project. M.E.A. made the crosses, set up the experimental pond and coordinated all field and laboratory research. M.E.A., K.B.M., S.K., N.B. and S.B. conducted fieldwork and stable-isotope analysis. M.D.M. measured functional morphological traits. B.M. and M.E.A. measured and analysed gut contents. S.K., D.S. and M.E.A. performed landmark-based morphometric analyses. M.E.A. analysed relationships between all traits and trophic variation. F.C.J., Y.F.C. and D.M.K. designed the SNP genotyping array. M.E.A., G.L.C., C.L.P and D.S. analysed SNP genotypes. D.S. determined the genealogy of the mapping population on the basis of SNP genotypes. M.E.A., C.L.P. and D.S. performed linkage and QTL analysis. M.E.A., C.L.P. and D.S. tested the genetic architecture of niche divergence. M.E.A., C.L.P., D.S., M.D.M., B.M. and G.L.C. interpreted the results. M.E.A. wrote the paper with input from C.L.P. and D.S., who are co-senior authors. All other authors provided editorial comments and approved the final version of the manuscript.

Author Information Reprints and permissions information is available at www.nature.com/reprints. The authors declare no competing financial interests. Readers are welcome to comment on the online version of the paper. Correspondence and requests for materials should be addressed to M.E.A. (marnegar@fhcrc.org).

METHODS

Experimental pond and F_2 hybrid population. We used an outdoor experimental pond at the University of British Columbia (Vancouver, Canada) containing shallow, littoral and deep, open-water habitats (Extended Data Fig. 1 and Supplementary Discussion). Four *in vitro* crosses were made between unique, wild-caught F_0 Paxton benthics and limnetics. F_0 females were benthic for two crosses and limnetic for the other two. After raising the F_1 families in separate aquariums[28], we stocked the pond on 17 March 2008 with five F_1 adults for each sex and family ($n = 40$). No food or nutrients were added to the pond after stocking (Supplementary Discussion). During these procedures, fin clips were removed from F_0 and F_1 individuals and stored in 95% ethanol for genetic analysis.

F_1 adults mated freely in the pond to produce an F_2 population. We collected 633 juvenile F_2 individuals in autumn 2008 (5–21 October), when rapid stickleback growth begins to slow[49] and before any overwintering mortality[25]. F_2 hybrids were captured with unbaited, fine-mesh minnow traps set in all parts of the pond. During fieldwork we selected 99 F_2 hybrids (in a blind manner) taken from traps deployed for no longer than 2 h. Each of these individuals was euthanized and preserved immediately for subsequent analysis of consumed food items in its digestive tract. All other individuals were housed in tanks and processed within 24 h. F_1 adults were readily excluded by size.

Niche use by F_2 juveniles. We euthanized F_2 hybrids with an overdose of buffered tricaine methanesulfonate and rinsed them in distilled water. Caudal and left pectoral fins were removed and stored in 95% ethanol for genetic analysis. Using a clean scalpel, we sampled white skeletal muscle from the posterior left flank, excluding any skin or bone, and immediately freeze-dried the samples in a BenchTop Manifold Freeze Dryer (Millrock Technology Inc.). Fish were fixed in 7.5% formalin (phosphate-buffered) for 1 month, and then transferred to 40% propan-2-ol.

We homogenized the freeze-dried muscle samples and took 0.8–1.2-mg subsamples, which were enclosed in tin capsules (Elemental Microanalysis Ltd), placed in 96-well microplates and stored in a vacuum-sealed desiccator. The subsamples were assayed for stable isotopes of carbon (^{12}C and ^{13}C) and nitrogen (^{14}N and ^{15}N) at the University of California, Davis, Stable Isotope Facility in one continuous run in January 2009. Measurements were made with a PDZ Europa ANCA-GSL elemental analyser interfaced to a PDZ Europa 20-20 mass spectrometer (Sercon Ltd); these are expressed as scaled isotope ratios, in parts per thousand (‰) relative to Pee Dee Belemnite or atmospheric N_2, using the standard delta notation ($\delta^{13}C$ or $\delta^{15}N$)[45,50]. We performed principal component analysis (PCA) on the bivariate isotope data using the function 'prcomp' in R (v.2.14.0)[51], after scaling both $\delta^{13}C$ and $\delta^{15}N$ to unit variance. The first PC axis (PC1, niche score) explained 56.5% of total variance in isotope space (first eigenvalue $\lambda_1 = 1.13$); PC2 (diet deviation score) explained the remaining 43.5% of variance ($\lambda_2 = 0.87$).

The $\delta^{13}C$ and $\delta^{15}N$ signature of skeletal muscle is an integrative measure of an individual's long-term diet (that is, several weeks to months)[17,45,50,52–57]. We compared these signatures with a direct measure of F_2 hybrid feeding activity immediately (that is, several hours) before capture, which we quantified by means of counts of ingested food items in 99 F_2 hybrids. Food items in the digestive tract of each individual were counted after being sorted into the following 14 categories: adult aquatic snails (class Gastropoda); snail eggs; ostracods (class Ostracoda); calanoid copepods, all identified as *Skistodiaptomus oregonensis* (order Calanoida); cyclopoid copepods (order Cyclopoida); *Chydorus* sp. (order Cladocera); *Sida* sp. (Cladocera); *Gammarus* sp. (order Amphipoda); water mites (unranked taxon Hydrachnidiae, suborder Prostigmata); caddisfly larvae (order Trichoptera); chironomid larvae (family Chironomidae); beetle larvae (order Coleoptera); springtails (order Symphypleona, subclass Collembola); and all other terrestrial and surface-dwelling (that is, neustonic) insects, combined. Four categories (chironomids, *S. oregonensis*, springtails and *Chydorus*) accounted for more than 98% of all ingested food items across individuals.

We used body size of fish at capture (length in millimetres) as a measure of feeding performance (Supplementary Discussion). Body size was taken as the distance between morphometric landmarks 1 and 13 (Extended Data Fig. 3). Size variation across the isotope landscape was visualized as the loess (local second-degree polynomial) regression surface of body size on $\delta^{13}C$ and $\delta^{15}N$, estimated using the R function 'loess'[51] (span = 0.75). A plot of this surface suggested isotopically distinct regions of extreme performance, reflected by especially large or small average body size of the juveniles in each region (Fig. 1a). To facilitate comparison of diet and morphology among regions, we used contours of the loess regression fit to establish boundaries around individuals of largest or smallest predicted body size. Each boundary was the most extreme predicted size contour enclosing a unique set of individuals numbering about 15% of the distribution ($n = 94$–95 per region). Thus, region B contained individuals of large average size near the performance peak at high $\delta^{13}C$ and low $\delta^{15}N$ (Fig. 1a), whereas region A contained individuals with the smallest average size observed overall, at low $\delta^{13}C$ and low $\delta^{15}N$. In these cases, the simple use of appropriate contours allowed a straightforward application of the 15% criterion. We wanted the third region (L) to also include individuals that grew to large average size (like region B) but were instead located around the performance peak at low $\delta^{13}C$ and high $\delta^{15}N$. With region L, however, a second criterion (minimization of PC1) was required to define a boundary that both contained an outer quantile (15%) of the predicted performance distribution and retained isotopic distinctiveness from other regions. Specifically, the boundary of region L was the maximum loess-predicted size contour enclosing 15% of the distribution (around the low-$\delta^{13}C$–high-$\delta^{15}N$ peak) after limiting this region to PC1 < 0.045. Next, we investigated variation in recent feeding activity among these categories of F_2 hybrids with Kruskal–Wallis tests (R function 'kruskal.test'[51]) for differences in counts of ingested food items (Fig. 1b–e).

To test the robustness of the performance valley at intermediate niche score (Fig. 1a), we fitted body size to niche score with a cubic spline function including F_2 family identity (indicating the offspring of each unique $F_1 \times F_1$ pairing) as a covariate. Doing so accounts for among-family variation in F_2 age at capture due to variable F_1 breeding times, assuming that unique F_1 pairs mated only once. Supporting this assumption, we found no deviations from unimodal size frequency distributions in F_2 families, judged by visual inspection and Hartigan's dip test[58] (R package 'diptest'[59]; 2,000 replicates per Monte Carlo simulation; each $P > 0.175$). Thus, cubic splines were estimated in 'glms' v.4.0 (http://www.zoology.ubc.ca/~schluter/wordpress/software/#spline)[48], using the 20 largest F_2 families (full sibs per family: $n = 12$–48). Using the best smoothing parameter (that is, λ with lowest cross-validation score), we obtained standard errors of predicted body sizes (1,000 bootstrap replicates). We also evaluated the robustness of the performance valley by quadratic regression of body size on niche score, again using the 20 largest families and the family identity covariate (Supplementary Discussion). The regression was repeated using only individuals for which PC2 < 0 to ensure that presence of the size valley did not depend solely on unusually small individuals with PC2 ≥ 0, including those in region A.

Morphological trait measurements. Three classes of morphological traits known to differ between wild Paxton benthics and limnetics (Supplementary Discussion) were measured: first, morphometric traits reflecting body shape; second, defensive armour traits; and third, single or composite functional traits (head and jaw) with described roles in feeding[16–19,60]. We measured shape by using the geometric morphometric approach of previous studies of sticklebacks[28,61]. Fixed specimens were stained for 48 h in 1% aqueous KOH with 0.005% w/v Alizarin Red S (Merck KGaA) and destained in 40% propan-2-ol. A Nikon D1H camera and three strobe lights were used to make a digital image of the right side of each specimen alongside a ruler. We recorded the x and y coordinates of 19 morphological landmarks from these images with 'tpsDig' v.2.12 (ref. 62) (Extended Data Fig. 3). We scaled, rotated and superimposed landmark configurations using Generalized Procrustes analysis[63] (R package 'shapes'[64]), after which we used a standard approach to correct for a specimen bending artefact caused by fixation[28,61,65] (Supplementary Discussion). The resulting x and y coordinates were treated as individual traits when analysing relationships between shape and stable isotopes and performing QTL mapping.

Images enabled the use of a simple ordinal scale for the rapid characterization of three armour traits: pelvic girdle (right side of body) and first and second dorsal spines. These traits received a score of 0 when absent, 2 when present, and 1 when expressed at an intermediate size between these two categories. 'Well-developed' lateral bony plates[16] were also counted along the right flank (that is, any plate whose height was judged to be at least one-third of the individual's body depth at that plate).

We measured functional morphological traits by using methods previously applied to sticklebacks[18,19,66]. Gill rakers on the left outer branchial arch were counted under a dissecting microscope after removal of the arch and associated cartilage from the opercular cavity. Any stained protuberance was counted as either a long or short gill raker according to position (Fig. 2e). After clearing specimens by immersion in 30% w/v sodium borate with 1% w/v trypsin until translucent, we measured five component traits of the suction feeding index[18,19] (Fig. 2f): anterior epaxial muscle height (E_H) and width (E_W), neurocranium outlever length (N_{OL}), buccal cavity length (B_L) and gape (G). Suction index was calculated as $(E_W E_H^2)/(3B_L G[N_{OL} - \frac{1}{2}B_L])$. Last, we measured upper jaw (premaxillary) protrusion length and lower jaw-opening inlever length (Fig. 2g)[19].

All functional morphological traits were corrected for body size (length) except long and short gill raker counts, which were uncorrelated with size. We used standardized major axis regression (function 'sma' in R package 'smatr'[67]) to test for differences in allometric scaling relationships of these traits between F_2 hybrids in the mapping population and wild Paxton benthics and limnetics. This revealed no evidence of allometric differences between the experimental fish and natural populations (likelihood ratio tests, 2 d.f. each: $0.09 < P < 0.56$). The traits were therefore size-corrected by expressing them as residuals from ordinary least-squares regression of each trait on body size[68].

Identifying 'component traits' of niche use. To determine which morphological traits predict variation along the primary trophic axis, we first regressed niche score on each trait separately by simple linear (least-squares) regression. Armour traits were excluded because we had no a priori evidence of specific influences on trophic variation (Supplementary Discussion). Similarly, we excluded suction feeding index, because each of its component traits was being considered. Scatterplots indicated that the data conformed reasonably well to parametric statistical assumptions. Only traits from the significant univariate regression models were considered further. Taking all such traits to be candidate explanatory variables, we performed all-subsets (multiple linear) regression[69] of niche score on the candidate traits, using the R function 'leaps'[70]. This function returns and orders the best models based on Mallows's C_P (ref. 71), which we converted to the Akaike information criterion (AIC)[72]. Because of partial redundancy between some of the functional traits and craniofacial landmarks, we considered functional morphology and shape trait classes separately when performing these exhaustive searches for trait subsets that best predicted niche score.

The difference between AIC scores of the 'best' (AIC = 0) and '*i*th best' models is denoted ΔAIC. We considered all models with $\Delta AIC \leq 2$ to be statistically indistinguishable from the overall 'best' model identified for given class of traits[73]. Consequently, the full suite of morphological traits for which this approach found similarly strong within-class evidence of an effect on niche score was the union of explanatory variables among all well-supported models ($0 < AIC \leq 2$) across the two trait classes (functional morphology and shape; Supplementary Tables 1 and 2, respectively). Hereafter we refer to this full suite of traits as the component traits of niche use. We repeated this entire procedure for identifying the morphological traits that influence a trophic axis, using diet deviation score as the response variable instead of niche score.

Genotyping and pedigree analysis. We isolated genomic DNA from fin tissue samples taken from the eight F_0 founders, 40 F_1 adults and 633 F_2 juveniles, using digestion with Proteinase K, extraction with phenol-chloroform and precipitation with ethanol[74]. We resuspended DNA in 30 μl of TE buffer (10 mM Tris, 1 mM EDTA, pH 8.0) and diluted an aliquot of each sample to a concentration of about 25 ng μl^{-1} based on PicoGreen assay (Life Technologies). All F_0 and F_1 individuals and 616 F_2 juveniles were genotyped at 408 SNP markers[30], which are distributed across the *G. aculeatus* genome and were polymorphic in our mapping population (Supplementary Table 4). Genotyping was performed with Illumina's GoldenGate assay at the Fred Hutchinson Cancer Research Center (Seattle, Washington, USA), using GenomeStudio software (Illumina Inc.) to score genotypes.

We used a Bayesian parentage assignment algorithm[75] (R package 'MasterBayes'[76]) and all SNP genotypes to estimate the F_1 parentage of every F_2 individual. Posterior probabilities of correct assignments of F_2 hybrids to their estimated pair of F_1 parents were high (mean ± s.d. 0.999 ± 0.020). Assignments of F_1 hybrids to known F_0 parents were verified (posterior probability = 1 in every case). Using a custom algorithm written in R, we then coded the SNP genotypes for linkage analysis and QTL mapping based on the reconstructed pedigrees for the F_2 hybrids.

Linkage analysis and QTL mapping. Among 728 F_2 hybrids collected in total from the experimental pond ($n = 633$ juveniles in this study; $n = 95$ adult males collected in spring 2009), we used all 594 genotyped individuals in F_2 families with at least ten full sibs (range 10–53 sibs per family) to construct a linkage map. This was done by using JoinMap v.3.0 ('cross pollinator' population code)[46]. All obtainable pairwise (between-SNP) recombination frequencies and associated $\log_{10}$ of odds (LOD) scores were computed separately for each F_2 family. We created a single pairwise data file by concatenating recombination frequencies and LOD scores across families and used this to produce the map (Supplementary Table 4).

We performed QTL mapping on all measured traits in R/qtl[47], using all F_2 families from the linkage analysis. Retaining all families after excluding F_2 hybrids collected in spring 2009 required a reduction in minimal acceptable family size (to eight full sibs). Accordingly, our data set for QTL mapping consisted of 530 F_2 hybrids in 29 F_2 families (range: 8–48 sibs per family). Using R/qtl function 'scanone' we performed interval mapping on each trait with Haley–Knott regression and F_2 family identity as a covariate. We conducted 10,000 permutations per trait to determine the genome-wide LOD threshold for significant QTLs at $\alpha = 0.05$ (ref. 47). The resulting LOD thresholds ranged from 3.51 to 3.88 across traits (mean 3.63). For every QTL, we estimated the position of the peak LOD score in centimorgans (cM) with a 1.5-LOD confidence interval around the peak[77]. R/qtl function 'fitqtl' was used to estimate the percentage of phenotypic variance explained by each QTL, and 'find.marker'[47] was used to identify the nearest SNP.

Genetic architecture of niche divergence. We investigated effects of the discovered morphological QTLs on niche divergence between Paxton benthics and limnetics as follows. First, we considered only QTLs underlying component traits of niche use. From these QTLs we selected the single QTL per LG with the highest LOD score among niche use component traits mapping to that LG. This procedure identified 14 candidate morphological QTLs (on different LGs) with hypothesized genetic effects on niche score. Repeating this procedure for 'diet deviation score', we identified 15 QTLs on different LGs with hypothesized effects on this secondary trophic axis.

To model cumulative effects of the 14 candidate QTLs on the niche score of F_2 hybrids, we specified candidate QTL positions by using R/qtl function 'makeqtl'. We then used 'fitqtl' to fit a MQM model of the main effects of the QTLs on niche score (Extended Data Table 2). Next, we found all significant pairwise QTL × QTL interactions among the candidate loci by applying the 'addint' function[47] to the 14 candidate QTLs. We added these interactions to the main-effects-only MQM model and performed backwards stepwise elimination of non-significant terms until arriving at the full MQM model (Extended Data Table 3). At every step, 'fitqtl' was used for model fitting with the Haley–Knott method and the F_2 family covariate.

We repeated this modelling procedure for diet deviation score and its 15 candidate QTLs. In this case we found nine significant QTL × QTL interactions by using 'addint', but these interactions were not accompanied by significant main effects (data not shown). Consequently, all further model comparisons were focused on testing genetic effects on niche score.

Using the full MQM model, we tested the importance of additive, dominance and pairwise epistatic effects in the genetic architecture of niche divergence between Paxton benthics and limnetics. In R/qtl we imputed genotypes at the SNP marker nearest to each QTL in this model using the Kosambi mapping function[78]. Subsequent model comparisons of QTL effects were performed with the linear model-fitting function 'lm'[51] in R. We specified the 'full' genetic model by coding genotypes as categorical data and including all additive, dominance and pairwise epistatic effects detected in R/qtl for the full MQM model (Extended Data Table 3). Using this genotype coding scheme, an 'additive + dominance' model was specified by including only genotype main effects from the 'full' model. In contrast, an 'additive' model was specified by coding genotypes in terms of the integer number of benthic alleles. Each model again included the F_2 family covariate. Models were compared by using AIC and adjusted R^2, which penalize models with excessive numbers of terms[72,73,79,80], and by using likelihood ratio tests (R function 'lrtest'[81]).

Animal care, sample size determination and data blinding. All field and laboratory procedures were approved by the University of British Columbia Animal Care Committee (protocols A07-0293 and A11-0402) and the Fred Hutchinson Cancer Research Center Institutional Animal Care and Use Committee (protocol 1797). The target sample size of F_2 hybrids was determined to minimize bias when detecting QTLs (the 'Beavis effect') and to reduce sampling error for estimated QTL effect sizes. Realized sample sizes for QTL mapping ($n = 473$–530 F_2 hybrids) were sufficient to minimize QTL detection bias and sampling error for effect sizes for every trait considered[47,82]. All reductions in sample size (from $n = 633$ juveniles collected) occurred in an unbiased fashion, because sample exclusion was based solely on missing phenotype or genotype data, or having too few full sibs in the collection. To avoid sampling and measurement biases, sample identities were not revealed to the authors and technicians who performed phenotypic measurements or genotyping until after all data collection had been completed. The 99 F_2 hybrids allocated for analysis of consumed food items were also selected in a blind manner during fieldwork.

Constructed to help clarify how the two-dimensional isotope distribution of F_2 hybrids related to other patterns of variation, F_2 groups B, L and A each contained about 15% of all F_2 hybrids collected. With the application of a second criterion minimizing PC1 scores in group L only, the 15% inclusion criterion yielded the largest number of individuals in each group without compromising group distinctiveness. Patterns of feeding and morphological variation among groups were robust to alternative body size thresholds (Supplementary Discussion), and they were confirmed by analyses using all individuals (Extended Data Fig. 2 and 6). Moreover, all available data were used for stable-isotope PCA, component trait determination, QTL analysis and genetic modelling; results of these analyses therefore did not depend on how F_2 hybrids were categorized to understand the performance landscape.

49. Wootton, R. J. *A Functional Biology of Sticklebacks* (Univ. of California Press, 1984).
50. Post, D. M. Using stable isotopes to estimate trophic position: models, methods, and assumptions. *Ecology* **83,** 703–718 (2002).
51. R. Development Core Team. *R: A Language and Environment for Statistical Computing* (http://www.R-project.org/) (R Foundation for Statistical Computing, 2011).
52. Vander Zanden, M. J. & Vadeboncoeur, Y. Fishes as integrators of benthic and pelagic food webs in lakes. *Ecology* **83,** 2152–2161 (2002).
53. Bolnick, D. I. *et al.* The ecology of individuals: incidence and implications of individual specialization. *Am. Nat.* **161,** 1–28 (2003).
54. McIntyre, P. B. & Flecker, A. S. Rapid turnover of tissue nitrogen of primary consumers in tropical freshwaters. *Oecologia* **148,** 12–21 (2006).
55. Harmon, L. J. *et al.* Evolutionary diversification in stickleback affects ecosystem functioning. *Nature* **458,** 1167–1170 (2009).
56. Behm, J. E., Ives, A. R. & Boughman, J. W. Breakdown in postmating isolation and the collapse of a species pair through hybridization. *Am. Nat.* **175,** 11–26 (2010).

57. Bolnick, D. I. Sympatric speciation in threespine stickleback: why not? *Int. J. Ecol.* **2011,** 942847 (2011).
58. Hartigan, J. A. & Hartigan, P. M. The dip test of unimodality. *Ann. Stat.* **13,** 70–84 (1985).
59. Maechler, M. *Package 'diptest': Hartigan's Dip Test Statistic for Unimodality*, corrected code, v. 0.75-4 (http://CRAN.R-project.org/package=diptest) (CRAN: Comprehensive R Archive Network, 2011).
60. Schluter, D. Adaptive radiation in sticklebacks: size, shape, and habitat use efficiency. *Ecology* **74,** 699–709 (1993).
61. Albert, A. Y. K. *et al.* The genetics of adaptive shape shift in stickleback: pleiotropy and effect size. *Evolution* **62,** 76–85 (2008).
62. Rohlf, F. J. *TpsDig2* (http://life.bio.sunysb.edu/morph/soft-dataacq.html) (Department of Ecology and Evolution, State Univ. of New York, 2006).
63. Rohlf, F. J. & Slice, D. Extensions of the Procrustes method for the optimal superimposition of landmarks. *Syst. Zool.* **39,** 40–59 (1990).
64. Dryden, I. L. *Package 'shapes': Statistical Shape Analysis*, v. 1.1-3 (http://CRAN.R-project.org/package=shapes) (CRAN: Comprehensive R Archive Network, 2009).
65. Arnegard, M. E. *et al.* Sexual signal evolution outpaces ecological divergence during electric fish species radiation. *Am. Nat.* **176,** 335–356 (2010).
66. Peichel, C. L. *et al.* The genetic architecture of divergence between threespine stickleback species. *Nature* **414,** 901–905 (2001).
67. Warton, D. I., Duursma, R. A., Falster, D. S. & Taskinen, S. SMATR 3—an R package for estimation and inference about allometric lines. *Methods Ecol. Evol.* **3,** 257–259 (2012).
68. Smith, R. J. Use and misuse of the reduced major axis for line-fitting. *Am. J. Phys. Anthropol.* **140,** 476–486 (2009).
69. Miller, A. *Subset Selection in Regression*, 2nd edn, Vol. 95 (Chapman & Hall/CRC, 2002).
70. Lumley, T. *Package 'leaps': Regression Subset Selection*, v. 2.9 (http://CRAN.R-project.org/package=leaps) (CRAN: Comprehensive R Archive Network, 2009).
71. Mallows, C. L. Some comments on C_P. *Technometrics* **15,** 661–675 (1973).
72. Akaike, H. A new look at the statistical model identification. *IEEE Trans. Automat. Contr.* **19,** 716–723 (1974).
73. Burnham, K. P. & Anderson, D. R. *Model Selection and Multimodel Inference: A Practical Information-Theoretic Approach*, 2nd edn (Springer, 2002).
74. Sambrook, J. & Russell, D. W. *Molecular Cloning: A Laboratory Manual*, 3rd edn (Cold Spring Harbor Laboratory Press, 2001).
75. Hadfield, J. D., Richardson, D. S. & Burke, T. Towards unbiased parentage assignment: combining genetic, behavioural and spatial data in a Bayesian framework. *Mol. Ecol.* **15,** 3715–3730 (2006).
76. Hadfield, J. *Package 'MasterBayes': ML and MCMC Methods for Pedigree Reconstruction and Analysis*, v. 2.50 (http://cran.r-project.org/web/packages/MasterBayes/) (CRAN: Comprehensive R Archive Network, 2012).
77. Manichaikul, A., Dupuis, J., Sen, S. & Broman, K. W. Poor performance of bootstrap confidence intervals for the location of a quantitative trait locus. *Genetics* **174,** 481–489 (2006).
78. Kosambi, D. D. The estimation of map distance from recombination values. *Ann. Eugen.* **12,** 172–175 (1944).
79. Theil, H. *Economic Forecasts and Policy*, 2nd edn (North-Holland, 1961).
80. Engle, R. F. & Brown, S. J. Model selection for forecasting. *Appl. Math. Comput.* **20,** 313–327 (1986).
81. Hothorn, T, *et al. Package 'lmtest': Testing Linear Regression Models*, v. 0.9-30 (http://CRAN.R-project.org/package=lmtest) (CRAN: Comprehensive R Archive Network, 2012).
82. Erickson, D. L., Fenster, C. B., Stenøien, H. K. & Price, D. Quantitative trait locus analyses and the study of evolutionary process. *Mol. Ecol.* **13,** 2505–2522 (2004).

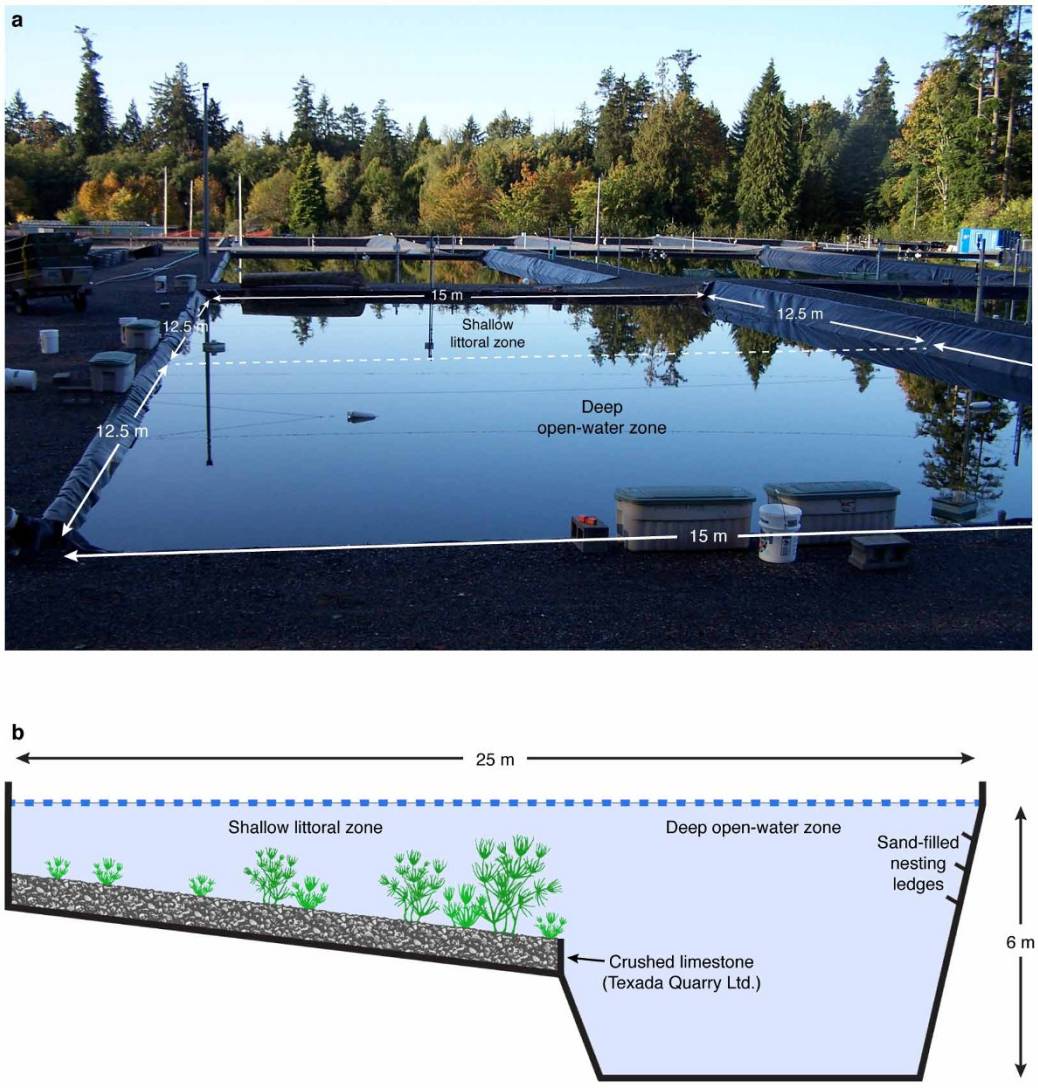

Extended Data Figure 1 | Experimental pond used in the study. **a**, Photograph of pond no. 4 at the experimental pond facility of the University of British Columbia (Vancouver, British Columbia, Canada), taken in autumn 2008, during the collection of F_2 juveniles. **b**, Diagram of the pond profile. See Supplementary Discussion for details on pond history before this study.

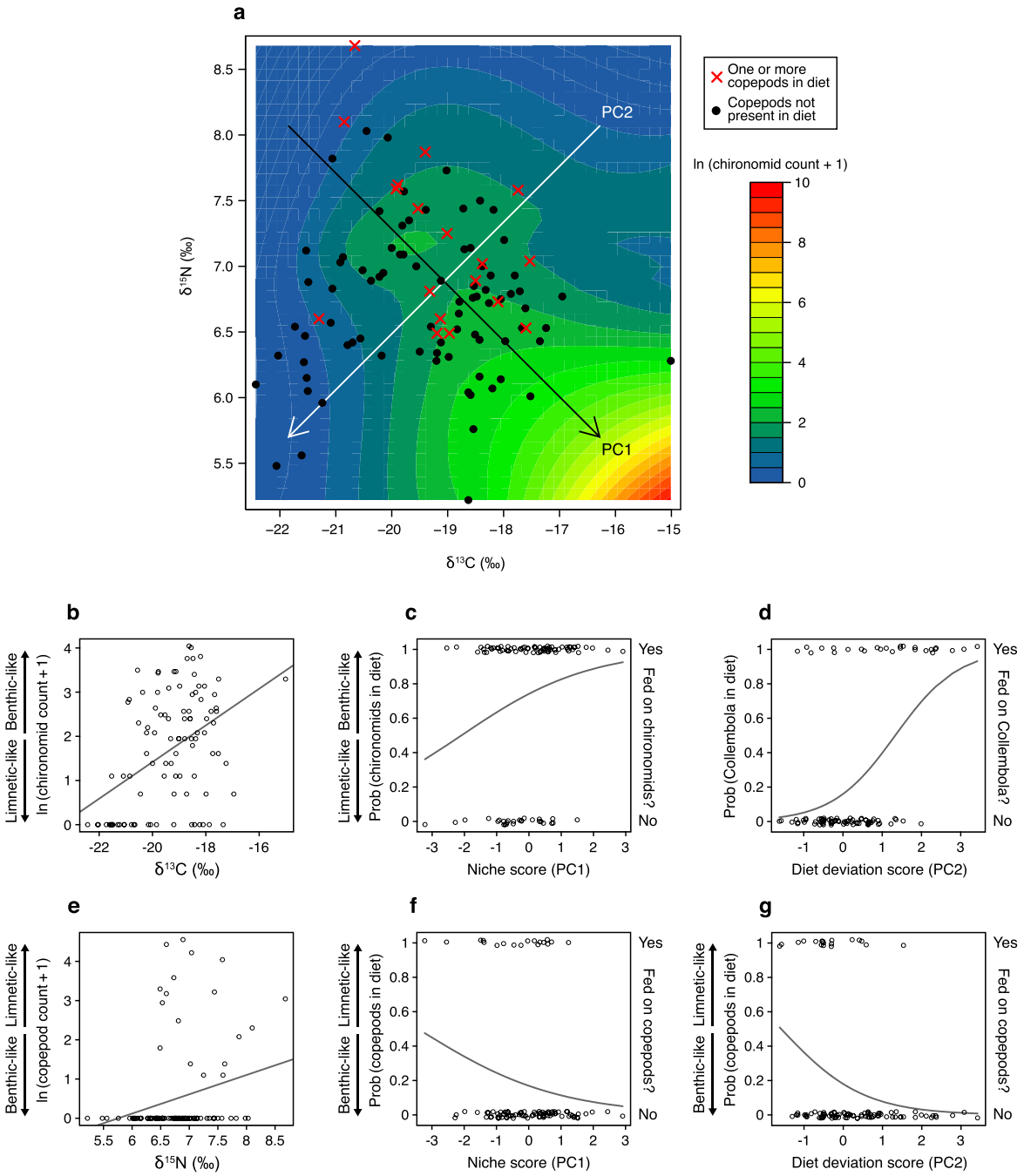

Extended Data Figure 2 | Feeding patterns in relation to isotope signatures. Plots show relationships between ingested prey counts from all available F_2 hybrids ($n = 99$) and stable-isotope data. **a**, Loess-smoothed surface (span = 0.75, second-degree polynomials) of predicted chironomid counts plotted on original isotope axes ($\delta^{13}C$, $\delta^{15}N$). As with all other count data plotted here, counts were transformed as ln (chironomids + 1) and mapped according to the coloured scale. PC1 (black arrow) and PC2 (white) are based on the entire isotope distribution (Fig. 1a). Individuals are plotted as points according to the presence (crosses) or absence (filled circles) of calanoid copepods in their digestive tracts. **b**–**g**, Linear or logistic regression, accordingly, of ingested prey count or presence/absence data (transformed as above) on the different axes through isotope space. **b**, Chironomid count against $\delta^{13}C$, linear regression, slope estimate = 0.415, $R^2 = 0.199$, $F_{1,97} = 24.1$, $P = 3.70 \times 10^{-6}$. **c**, Chironomid presence against niche score, logistic regression, slope coefficient = 0.504, $z = 2.23$, $P = 0.0255$. **d**, Collembola presence against diet deviation score, logistic regression, slope coefficient = 1.25, $z = 4.26$, $P = 2.03 \times 10^{-5}$. **e**, Calanoid copepod count against $\delta^{15}N$, linear regression, slope estimate = 0.492, $R^2 = 0.0608$, $F_{1,97} = 6.28$, $P = 0.0139$. **f**, Calanoid copepod presence against niche score, logistic regression, slope coefficient = −0.463, $z = -1.84$, $P = 0.0651$. **g**, Calanoid copepod presence against diet deviation score, logistic regression, slope coefficient = −0.958, $z = -2.67$, $P = 0.00766$.

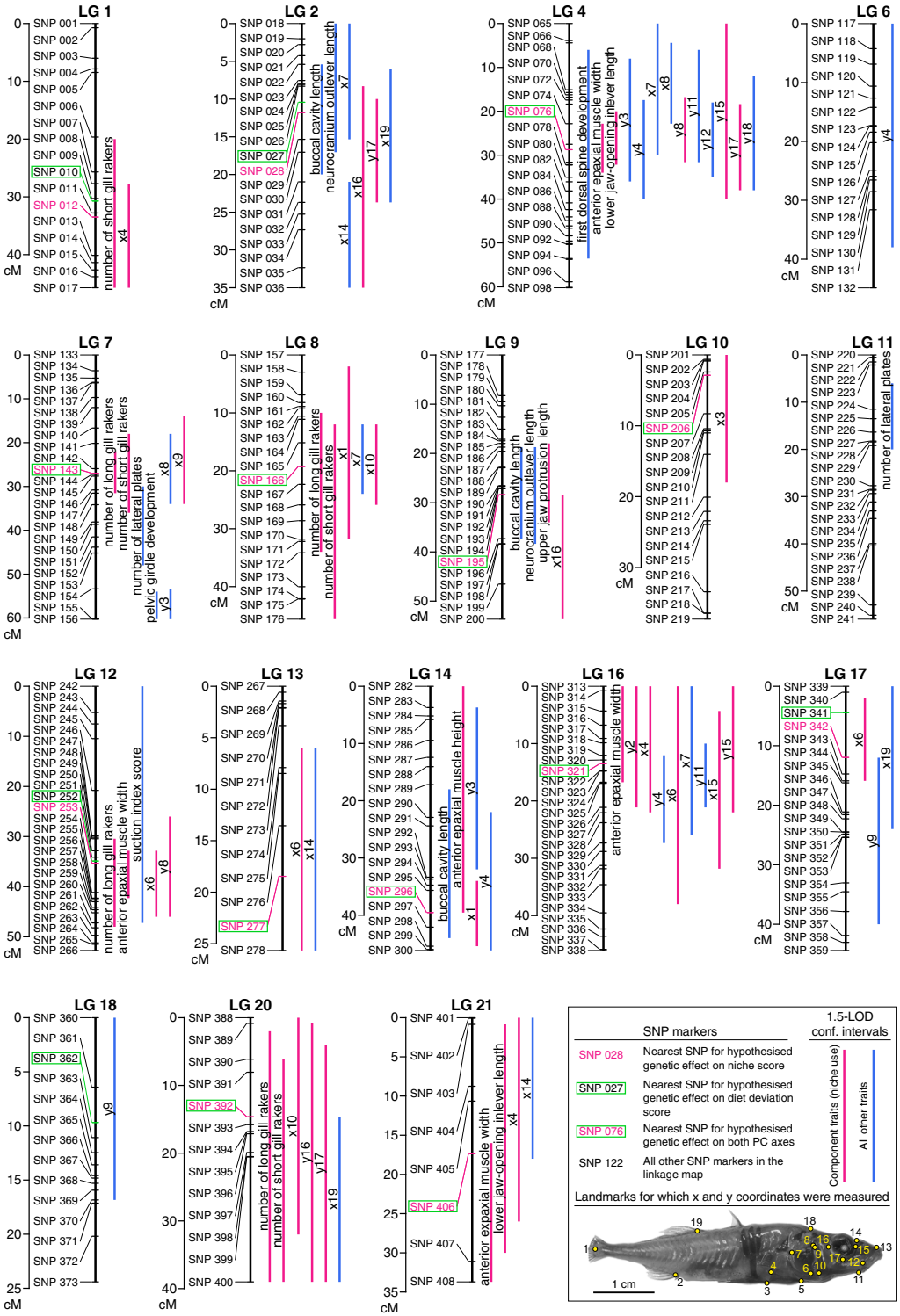

Extended Data Figure 3 | Linkage map showing QTLs for all traits. All *G. aculeatus* chromosomes are represented by LGs in the complete linkage map for this study (LGs and chromosomes use the same numbering[29]; LGs with no mapped QTLs are omitted here). Map distances are indicated with a scale at the left of each LG in centimorgans (cM). Coloured bars (at the right) are 1.5-LOD confidence intervals for QTL position (red bars, component traits of niche use; blue bars, other traits; Supplementary Table 3 provides LOD scores, map positions of LOD peaks, and effect sizes). The given SNP identifiers (IDs) are only for reference to Supplementary Table 4, which provides published SNP data[30]. For clarity, every other ID is omitted for SNP 066–098, even though these markers are present in the map. Markers closest to candidate QTLs for genetic model comparisons are highlighted: red text, nearest to candidate QTLs for niche score; green boxes, diet deviation score. Numbered traits are the *x* and *y* coordinates of morphometric landmarks (indicated on the fish photo): 1, posterior midpoint caudal peduncle; 2, anterior insertion anal fin at first soft ray; 3, posteroventral corner ectocoracoid; 4, posterodorsal corner ectocoracoid; 5, anteriormost corner ectocoracoid; 6, anteroventral corner opercle; 7, posterodorsal corner opercle; 8, dorsal edge opercle–hyomandibular boundary; 9, dorsalmost extent preopercle; 10, posteroventral corner preopercle; 11, anteriormost extent preopercle along ventral silhouette; 12, posteroventral extent maxilla; 13, anterodorsal extent maxilla; 14, suture between nasal and frontal bones along dorsal silhouette; 15, anterior margin orbit; 16, posterior margin orbit; 17, ventral margin orbit (landmarks 15–17 placed in line with vertical or horizontal midpoint of eye); 18, posterior extent supraoccipital along dorsal silhouette; 19, anterior insertion dorsal fin at first soft ray.

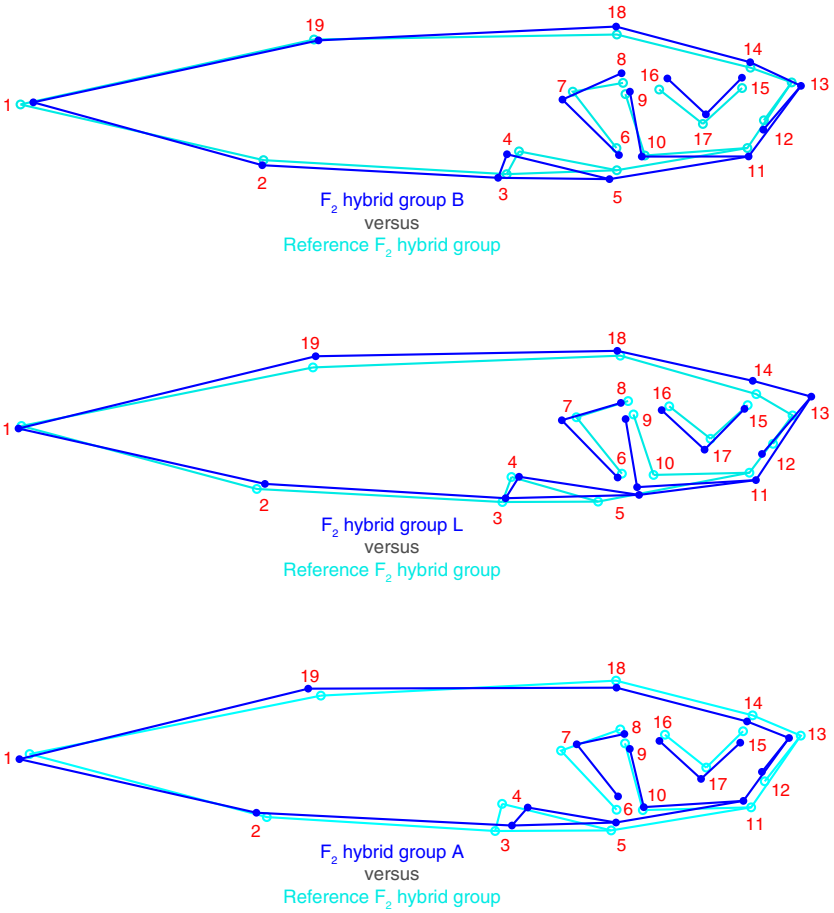

Extended Data Figure 4 | Shape variation among F_2 hybrid groups. Each overlaid pair of wireframe diagrams compares the mean body shape of individuals in one of three groups of F_2 hybrids (B, L or A; shown in dark blue) with the relative mean shape of a reference group consisting of all other F_2 hybrids (group membership shown in Fig. 1a). Using data for 19 Procrustes-superimposed and unbent landmarks (Extended Data Fig. 3), the wireframe diagrams were produced and plotted in MorphoJ v.1.04a, on the basis of discriminant function analysis (Supplementary Discussion). The shape differences represented here are magnified eightfold for easier visual comparison. Group sample sizes: $n = 91$ (B), $n = 92$ (L), $n = 93$ (A), $n = 335$ (reference group). See Supplementary Discussion for a detailed description of patterns of variation in several specific features of shape that can be interpreted from these data.

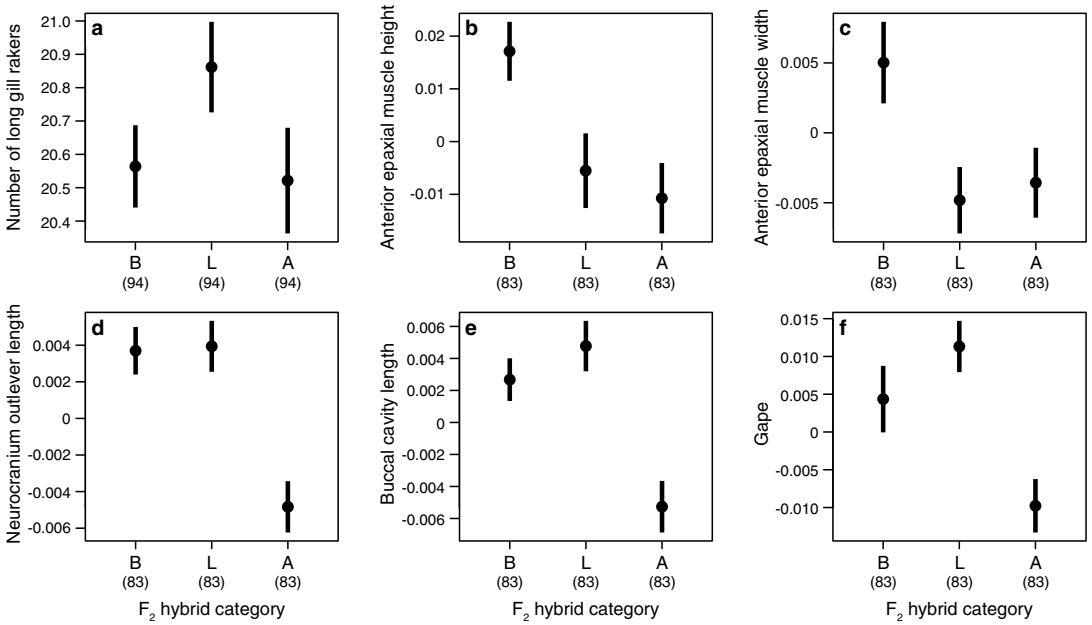

Extended Data Figure 5 | Variation of additional traits among F_2 hybrid groups. Means ($\pm$ 1 s.e.m.) of F_2 hybrids in groups B, L and A (Fig. 1a) are shown for the following traits (using raw data for long gill rakers and size-corrected data for the other traits): **a**, number of long gill rakers (ANOVA, $F_{2,279} = 1.756$, $P = 0.175$); **b**, residual anterior epaxial muscle height ($F_{2,246} = 5.219$, $P = 0.00603$); **c**, residual anterior epaxial muscle width ($F_{2,246} = 4.223$, $P = 0.0157$); **d**, residual neurocranium outlever length ($F_{2,246} = 13.36$, $P = 3.10 \times 10^{-6}$); **e**, residual buccal cavity length ($F_{2,246} = 12.26$, $P = 8.42 \times 10^{-6}$); **f**, residual gape ($F_{2,246} = 7.974$, $P = 4.41 \times 10^{-4}$). Numbers in parentheses are values of *n*. Traits are illustrated in Fig. 2e–g. The data conformed reasonably well to parametric statistical assumptions; ANOVA was therefore used to test trait variation among categories.

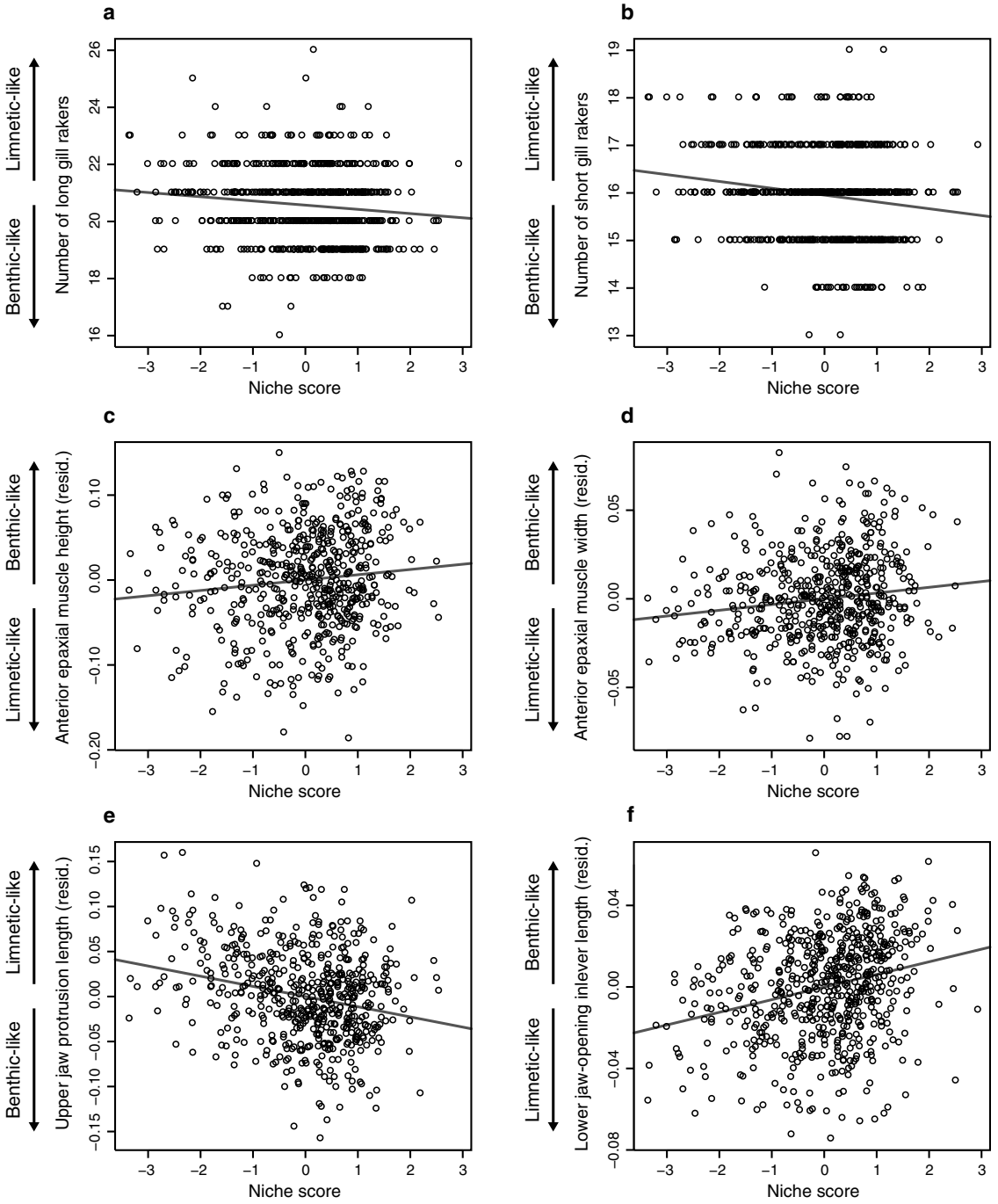

Extended Data Figure 6 | Relationships between F_2 hybrid functional morphology and niche score. For key functional morphological traits known to differ between wild Paxton benthics and limnetics, trait data from all available F_2 hybrids are plotted against niche score and fitted with linear regression (raw data for gill raker counts; size-corrected data for other traits): **a**, number of long gill rakers ($R^2 = 0.0146$; $F_{1,629} = 9.32$; $P = 0.00236$); **b**, number of short gill rakers ($R^2 = 0.0253$; $F_{1,629} = 16.30$; $P = 6.06 \times 10^{-5}$); **c**, residual anterior epaxial muscle height ($R^2 = 0.0125$; $F_{1,552} = 7.00$; $P = 0.00804$); **d**, residual anterior epaxial muscle width ($R^2 = 0.0189$; $F_{1,552} = 10.61$; $P = 0.00119$); **e**, residual upper jaw protrusion length ($R^2 = 0.0580$; $F_{1,552} = 34.00$; $P = 9.40 \times 10^{-9}$); **f**, residual lower jaw-opening inlever length ($R^2 = 0.0660$; $F_{1,615} = 43.43$; $P = 9.45 \times 10^{-11}$). Traits are illustrated in Fig. 2e–g. Directions of benthic–limnetic divergence in Paxton Lake (arrows at left of plots, here and in Fig. 2a–d) are based on previously published studies[16,18,19], combined with validating counts of long and short gill rakers for this study (data not shown).

Extended Data Table 1 | Goodness-of-fit tests for genomic distribution of QTLs

LG	Size (b.p.)	Percentage of assembled genome's size	Coding + non-coding genes	Percentage of total count of coding + non-coding genes	QTL for all traits	Percentage of total QTL count (all traits)	QTL for component traits only	Percentage of total QTL count (component traits)
1	28,185,914	7.033 %	1,257	6.581 %	2	2.632 %	2	4.878 %
2	23,295,652	5.812 %	860	4.502 %	7	9.210 %	2	4.878 %
3	16,798,506	4.191 %	932	4.880 %	0	0 %	0	0 %
4	32,632,948	8.142 %	1,323	6.926 %	13*,†	17.105 %	5	12.195 %
5	12,251,397	3.057 %	732	3.832 %	0	0 %	0	0 %
6	17,083,675	4.263 %	721	3.775 %	1	1.316 %	0	0 %
7	27,937,443	6.970 %	1,320	6.911 %	7	9.210 %	3	7.317 %
8	19,368,704	4.833 %	881	4.612 %	5	6.579 %	4	9.756 %
9	20,249,479	5.052 %	1,012	5.298 %	4	5.263 %	2	4.878 %
10	15,657,440	3.907 %	815	4.267 %	1	1.316 %	1	2.439 %
11	16,706,052	4.168 %	1,058	5.539 %	1	1.316 %	0	0 %
12	18,401,067	4.591 %	1,003	5.251 %	5	6.579 %	4	9.756 %
13	20,083,130	5.011 %	970	5.078 %	2	2.632 %	1	2.439 %
14	15,246,461	3.804 %	736	3.853 %	5	6.579 %	2	4.878 %
15	16,198,764	4.042 %	778	4.073 %	0	0 %	0	0 %
16	18,115,788	4.520 %	801	4.194 %	9*,†	11.842 %	6*,†	14.634 %
17	14,603,141	3.644 %	702	3.675 %	3	3.947 %	1	2.439 %
18	16,282,716	4.063 %	762	3.989 %	1	1.316 %	0	0 %
19	20,240,660	5.050 %	1,044	5.466 %	0*,†	0 %	0	0 %
20	19,732,071	4.923 %	931	4.874 %	6	7.895 %	5*,†	12.195 %
21	11,717,487	2.924 %	463	2.424 %	4	5.263 %	3†	7.317 %
Sum	400,788,495‡	100 %	19,101§	100 %	76	100 %	41	100 %

Expected numbers of QTLs on LGs, under a random-distribution null hypothesis (simple proportional model), were based on the known size (second column from the left) and gene content (fourth column; predicted number of coding plus non-coding genes) of corresponding chromosomes (obtained from Ensembl genome browser on 17 July 2013; based on initial *G. aculeatus* assembly, Broad S1, February 2006). Observed numbers and percentages of QTLs for all measured traits or only component traits are given in the last four columns (at the right). Results of all tests support the alternative hypothesis of QTL clustering: $\chi^2_{20} = 45.17$, $P = 0.0016$ (for all traits, with a null expectation based on chromosome size); $\chi^2_{20} = 55.76$, $P = 0.0002$ (all traits, based on gene number); $\chi^2_{20} = 34.87$, $P = 0.0219$ (component traits, based on chromosome size); $\chi^2_{20} = 39.12$, $P = 0.0083$ (component traits, based on gene number); P values were estimated by Monte Carlo simulation (10,000 replicates each) because of small expected counts for many LGs. Standardized residuals were used to identify LGs with QTL counts deviating from random expectation (Supplementary Discussion): $*P < 0.05$ (expectation based on chromosome size); $\dagger P < 0.05$ (gene content). Sums for size (‡) and gene content (§) exclude unassembled regions of the genome.

Extended Data Table 2 | MQM model of only main effects of 14 candidate morphological QTLs on niche score

Model term	Map location (cM)	Nearest SNP	PVE	*F*	d.f.	*P*-value (*F*)
LG1	36.00	chrI:25560380	0.52 %	1.688	2	0.185991
LG2†	12.00	chrII:10092618	1.69 %	5.470	2	0.004480†
LG4‡	28.76	chrIV:10997988	2.34 %	7.542	2	0.000596‡
LG7‡	26.99	chrVII:19857837	3.28 %	10.58	2	3.21×10^{-05}‡
LG8‡	18.00	chrVIII:16299555	3.74 %	12.08	2	7.63×10^{-06}‡
LG9	28.38	chrIX:6126845	0.84 %	2.719	2	0.066968
LG10	4.00	chrX:1275840	0.66 %	2.121	2	0.121029
LG12	38.00	chrXII:15046849	0.57 %	1.846	2	0.159010
LG13*	20.00	chrXIII:17392141	1.16 %	3.733	2	0.024619*
LG14	39.55	chrXIV:4632223	0.24 %	0.776	2	0.460631
LG16†	13.52	chrXVI:9981125	2.16 %	6.989	2	0.001020†
LG17	12.00	chrXVII:2232080	0.03 %	0.109	2	0.896894
LG20*	14.62	chrXX:9279241	1.43 %	4.630	2	0.010198*
LG21	18.00	chrXXI:11060209	0.33 %	1.080	2	0.340247

The table summarizes a main effects-only MQM model enforced to contain all the selected candidate morphological QTLs for niche score (run in R/qtl: niche score as response variable, Haley–Knott regression, with F_2 family covariate). Model terms (at the left) are named according to LG locations of the candidate QTLs, which were limited to the one best candidate for each LG before modelling (see Methods). For each QTL (model term), the table also gives the map position in centimorgans (cM), the nearest SNP marker, the percentage of total variance explained (PVE) for niche score, the *F*-test statistic, the corresponding degrees of freedom (d.f.), and the *P* value. Significant model terms are indicated as follows: *$0.01 \leq P < 0.05$; †$0.001 \leq P < 0.01$; ‡$P < 0.001$. Overall model results (SS, sum of squares): $SS_{model} = 169.34$; $d.f._{model} = 56$; $SS_{error} = 464.09$; $d.f._{error} = 473$; $LOD_{model} = 35.80$; $PVE_{model} = 26.73\%$; *P* value (*F*) $= 2.91 \times 10^{-11}$.

Extended Data Table 3 | Full MQM model of main QTL effects and effects of pairwise QTL interactions on niche score

Model term	PVE	*F*	d.f.	*P*-value (*F*)
LG1†	3.02 %	3.486	6	0.00222†
LG2†	1.50 %	5.200	2	0.00584†
LG4‡	4.30 %	4.958	6	6.21×10^{-05}‡
LG7‡	4.63 %	5.341	6	2.40×10^{-05}‡
LG8‡	3.48 %	12.04	2	7.97×10^{-06}‡
LG9*	0.96 %	3.328	2	0.03672*
LG13*	1.18 %	4.099	2	0.01720*
LG14*	1.90 %	2.192	6	0.04268*
LG16‡	5.57 %	3.858	10	4.87×10^{-05}‡
LG17†	3.95 %	2.737	10	0.00278†
LG20†	1.43 %	4.956	2	0.00742†
LG1xLG16†	2.48 %	4.284	4	0.00205†
LG4xLG17†	1.99 %	3.440	4	0.00873†
LG7xLG17*	1.54 %	2.658	4	0.03233*
LG14xLG16*	1.36 %	2.414	4	0.04817*

The table summarizes the final MQM model of candidate QTL effects on niche score, obtained by the stepwise model selection procedure described in Methods. At all steps, model fitting was performed in R/qtl (niche score as response variable, Haley–Knott regression, with F_2 family covariate). Model terms (at the left) are named according to the LG locations of candidate morphological QTLs (map positions in Extended Data Table 2). For each term (QTL), the table also gives the PVE for niche score, the *F*-test statistic, the corresponding degrees of freedom (d.f.), and the *P* value. Significant model terms are indicated as follows: $*0.01 \leq P < 0.05$; $\dagger 0.001 \leq P < 0.01$; $\ddagger P < 0.001$. Overall model results (SS, sum of squares): $SS_{model} = 209.75$; $d.f._{model} = 66$; $SS_{error} = 423.68$; $d.f._{error} = 463$; $LOD_{model} = 46.28$; $PVE_{model} = 33.11\%$; *P* value (F) $= 3.44 \times 10^{-15}$.